Lipids in Health and Disease

RESEARCH

Open Access

Exploring the molecular mechanisms of tirzepatide in alleviating metabolic dysfunction-associated fatty liver in mice through integration of metabolomics, lipidomics, and proteomics

Jinliang Liang[1†], Huanyi Liu[1†], Guo Lv[1†], Xiaotong Chen[1], Zhaoshou Yang[2], Kunhua Hu[1*] and Hongyan Sun[3*]

Abstract

Clinical studies have suggested that tirzepatide may also possess hepatoprotective effects; however, the molecular mechanisms underlying this association remain unclear. In our study, we performed biochemical analyses of serum and histopathological examinations of liver tissue in mice. To preliminarily explore the molecular mechanisms of tirzepatide on metabolic dysfunction-associated fatty liver disease (MAFLD), liquid chromatography-mass spectrometry (LC-MS) was employed for comprehensive metabolomic, lipidomic, and proteomic analyses in MAFLD mice fed a high-fat diet (HFD). The results demonstrated that tirzepatide significantly reduced serum levels of alanine transaminase (ALT) and aspartate transaminase (AST), as well as hepatic triglycerides (TG) and total cholesterol (TC), indicating its efficacy in treating MAFLD. Further findings revealed that tirzepatide reduced fatty acid uptake by downregulating Cd36 and Fabp2/4, as well as enhance the mitochondrial-lysosomal function by upregulating Lamp1/2. In addition, tirzepatide promoted cholesterol efflux and reduced cholesterol reabsorption by upregulating the expression of Hnf4a, Abcg5, and Abcg8. These results suggest that tirzepatide exerts its therapeutic effects on MAFLD by reducing fatty acid uptake, promoting cholesterol excretion, and enhancing mitochondrial-lysosomal function, providing a theoretical basis for a comprehensive understanding of tirzepatide.

Keywords Metabolic dysfunction-associated fatty liver disease, Tirzepatide, Metabolomics, Lipidomics, Proteomics

†Jinliang Liang, Huanyi Liu and Guo Lv contributed equally to this work.

*Correspondence:
Kunhua Hu
hukunh@mail.sysu.edu.cn
Hongyan Sun
sunhy@sysucc.org.cn

[1]Guangdong Provincial Key Laboratory of Liver Disease Research, The Third Affiliated Hospital of Sun Yat-sen University, Guangzhou 510630, China
[2]The First Affiliated Hospital, The First School of Clinical Medicine of Guangdong Pharmaceutical University, Guangdong Pharmaceutical University, Guangzhou 510080, China
[3]The State Key Laboratory of Oncology in South China, Sun Yat-Sen University Cancer Center, Guangzhou 510060, China

Introduction

Metabolic dysfunction-associated fatty liver disease (MAFLD) is widely recognised as a major cause of chronic liver disease, affecting nearly 30% of the global population [1]. Its prevalence is escalating annually, driven by the increasing incidence of obesity and type 2 diabetes [2, 3]. MAFLD triggers a spectrum of liver disorders, from simple hepatic steatosis (MAFLD) to more advanced metabolic dysfunction-associated steatohepatitis (MASH), which can progress to liver fibrosis, cirrhosis, liver failure, and hepatocellular carcinoma [4, 5]. Moreover, accumulating evidence suggests that MAFLD has systemic repercussions escalated with cardiovascular disease, chronic kidney disease, and various extrahepatic malignancies [6, 7]. Current treatment options for MAFLD focus primarily on lifestyle interventions, such as dietary changes and physical activity, which pose challenges for long-term adherence owing to the difficulty in maintaining these lifestyle changes over time. These underscore the urgent need for effective therapeutic strategies for MAFLD.

Recently, there have been notable progress in the field of metabolic diseases, particularly in the demonstrated therapeutic potential of glucagon-like peptide-1 (GLP-1) and glucose-dependent insulinotropic peptide (GIP) receptor agonists [8]. These peptides have been shown to effectively reduce hepatic steatosis in preclinical models [9–13]. Tirzepatide, a dual GIP/GLP-1 receptor agonist, has been approved for the management of type 2 diabetes and obesity [14], demonstrating superior efficacy in terms of glycemic control and weight reduction compared with monospecific receptor agonists [15, 16]. The dual-action mechanism of tirzepatide makes it a candidate for treating MAFLD, a condition intimately associated with metabolic dysregulation.

Although preclinical and clinical data are promising, the detailed molecular mechanisms by which tirzepatide influences MAFLD remain unclear. Recent research has shed light on the roles of GIPR and GLP1R agonists in the regulation of postprandial lipid metabolism [17–19] and inflammatory responses [20, 21]; however, the mechanisms of action of tirzepatide in MAFLD have not been extensively investigated. Therefore, a thorough examination of the molecular mechanisms of tirzepatide in MAFLD is essential to elucidate the mechanism of action of this drug and establish a foundation for the development of targeted therapeutic strategies for MAFLD.

The incorporation of multiomics technologies has significantly enhanced our understanding of complex biological systems and their regulatory mechanisms [22]. Advances in mass spectrometry (MS), particularly in proteomics and metabolomics, have provided robust tools for exploring the molecular mechanisms underlying various diseases. In this study, we used ultra-performance liquid chromatography coupled with Orbitrap tandem mass spectrometry (UPLC-Orbitrap-MS/MS) for comprehensive metabolomics, lipidomics, and proteomics analyses with the aim of elucidating the potential molecular mechanisms through which tirzepatide alleviates MAFLD in mice fed a high-fat diet (HFD). This innovative approach provides scientific evidence for the application of tirzepatide in MAFLD treatment and highlights its transformative potential in managing this prevalent liver disorder.

Methods

Animal model

29 Male C57BL/6J mice, aged 5 weeks, were procured from Guangdong Gempharmatech Co., Ltd. (Guangzhou, China). Housed in an SPF-certified facility, all mice were subjected to a consistent 12-h light/dark cycle, with a stable temperature of 24 °C (± 2) and humidity level of approximately 60% (± 10%). After a 7-d acclimatisation phase, the subjects were assigned to two distinct dietary groups: a normal diet group (NCD group, $n = 10$) and an HFD group ($n = 19$; diet obtained from Dyets, HF60, 60% calories from fat). Following a 20-week nutritional protocol, the HFD group was further subdivided into two groups: the HFD control group (HFD, $n = 9$) and the tirzepatide intervention group (HFD + tirzepatide, $n = 10$). The mice in the intervention group received subcutaneous injections of tirzepatide (Eli Lilly and Company, Indianapolis, Indiana) with dose escalation: initially, 0.03 mg/kg for the first 4 weeks, followed by 0.1 mg/kg for the subsequent 4 weeks, culminating at 0.3 mg/kg for the final 4 weeks, with administrations twice weekly. Counterparts of the NCD and HFD groups were administered placebo with 40 mM Tris-HCl buffer. During the investigational period at week 32, the mice were sedated via an intraperitoneal injection of pentobarbital sodium (40 mg/kg) for humane euthanasia. Blood and liver samples were collected for subsequent examination.

Analysis of the fatty liver model

Following a 20-week period of the specified dietary protocol, the mice were subjected to in-depth ultrasound assessment of their liver tissue using a Vevo 3100 system (FUJIFILM Visual Sonics, Toronto, Canada). The ultrasound results were analysed via the Vevo Lab software (FUJIFILM VisualSonics, Toronto, Canada) to compare the brightness of the ultrasound scans between the liver and kidneys, enabling the evaluation of lipid deposition in the liver.

Biochemical analysis

Serum was isolated from blood samples by centrifugation, and the concentrations of alanine transaminase (ALT), aspartate transaminase (AST), triglycerides (TG),

total cholesterol (TC), high-density lipoprotein cholesterol (HDL-C), and low-density lipoprotein cholesterol (LDL-C) were quantified via a 7180-ISE automated biochemical analyser (Hitachi, Tokyo, Japan).

Histopathological analysis

The liver samples were preserved in 10% paraformaldehyde, sectioned, and embedded in paraffin via standard procedures. Paraffin-embedded tissues were cut into 5-μm sections and stained with haematoxylin and eosin (HE). In addition, liver tissues embedded in OCT were cut into 10-μm sections and stained with Oil Red O (ORO). The stained sections were then scanned via the Tissue FAXS SL Spectra imaging system (Tissue Gnostics, Vienna, Austria). Finally, t Strata Quest software (Tissue Gnostics, Vienna, Austria) was employed to quantify lipid deposition areas and calculate the percentage of lipid deposition (ORO staining).

Untargeted metabolomic and lipidomic analyses

Fresh liver tissues (50 mg) were homogenised with 1 mL of ice-cold extraction solvent (methanol: water = 4:1 v/v; containing 3 μg/mL[13 C-methyl]-L-methionine as an internal standard). The homogenate was centrifuged at 14,000 rpm for 10 min at 4 °C, and the supernatant (850 μL) was collected and transferred to Eppendorf tubes. These supernatants were stored at -20 °C overnight, followed by a second centrifugation at 14,000 rpm for 10 min at 4 °C to remove residual particles. Appropriate volumes of all samples were pooled for quality control (QC). Lipid extraction involved adding 1 mL of ice-cold solvent (methyl tert-butyl ether: methanol = 10:3) to the precipitate from the initial centrifugation, homogenising, standing at room temperature for 30 min, and centrifuging at 14,000 rpm for 10 min at 4 °C. The resulting supernatants (400 μL) were concentrated under vacuum at room temperature and reconstituted in 120 μL of acetonitrile/water (1:1). A final centrifugation at 14,000 rpm for 10 min at 4 °C ensured particle removal, with a QC sample prepared by pooling appropriate volumes from all samples.

Untargeted metabolomic and lipidomic analyses were performed via a UHPLC U3000 system coupled with a QE HF-X mass spectrometer (Thermo Fisher Scientific, Waltham, MA, USA). Polar compounds were separated via an HILIC column (Agilent ZORBAX HILIC Plus, 3.0 mm × 100 mm, 1.8 μm), and lipid compounds were separated via a C18 column (Thermo Hypersil Gold C18, 2.1 mm × 100 mm, 1.9 μm). The mobile phases for the HILIC positive-ion mode consisted of 95% acetonitrile with 5 mM ammonium formate and 0.1% formic acid (A), and 50% acetonitrile containing 5 mM ammonium formate and 0.1% formic acid (B). In HILIC negative-ion mode, the mobile phases were 95% acetonitrile with 5 mM ammonium formate (A) and 50% acetonitrile containing 5 mM ammonium formate (B). The C18 reverse-phase analysis was performed using solvents A (acetonitrile: water = 6:4, 2 mM ammonium formate) and B (acetonitrile : isopropanol = 1 : 9, 2 mM ammonium formate). The ion source parameters included a spray voltage of -2.8 kV for negative polarity and + 3.5 kV for positive polarity. The spectral resolution was set to 120,000 for the full mass and 15,000 for the dd mass. The mass spectral acquisition ranged from 70 to 1050 Da.

Proteomic analysis

Tissue samples (20 mg) were homogenised in a buffer containing 50 mM Tris-HCl, 50 mM NaCl (pH 8.0), 1% NP-40, 0.1% SDS, and a protease and phosphatase inhibitor cocktail (Thermo Fisher Scientific). The homogenate was clarified by ultracentrifugation, and the supernatant was used for BCA protein concentration measurements. Proteins were reduced with 10 mM TCEP and alkylated with 25 mM IAM. Following protein precipitation, the samples were reconstituted in 100 mM TEAB with 8 M urea (pH 8.0), and subsequently diluted with eight volumes of 100 mM TEAB to reduce the urea concentration below 1 M. Trypsin was added at an enzyme-to-substrate ratio of 1:50 overnight digestion at 37 °C. After digestion, the peptides were desalted, dried, and reconstituted in 0.1% formic acid. Peptide concentrations were measured via a NanoDrop spectrophotometer (Thermo Fisher Scientific) and iRT peptides (Biognosys, Schlieren, Switzerland) were used for LC-MS/MS analysis.

Chromatographic separation was performed as previously described. The samples (1.5 μL) were loaded onto a trap column (Acclaim PepMap 100, 75 μm × 20 mm, C18) and then separated on an analytical column (75 μm × 250 mm, C18, 1.9 μm) via a 110-min gradient of A (acetonitrile : water = 4 : 1; 0.1% formic acid) (5–80%) and B (water; 0.1% formic acid) at a flow rate of 400 nL/min. The Q Exactive HF-X mass spectrometer was operated in the data-independent acquisition (DIA) mode, with each cycle comprising one full scan and 23 DIA scans covering a mass range of 300–1200 Th. The full scan was set to a resolution of 60,000 with an AGC target of 3e6 and an IT of 50 ms, followed by DIA scans with a resolution of 30,000 and an NCE set to 30.

Validation experiment based on parallel reaction monitoring (PRM)

To further validate our proteomics data, we selected proteins related to lipid synthesis (Cd36, Fabp2, Fabp4, Plin2, Plin4, and Plin5), fatty acid oxidation (FAO) (Cpt1a, Acaa1b, and Cyp4a10), the mitophagy-lysosome pathway (Bnip3, Sqstm1, Optn, Map1lc3b, Lamp1, Lamp2, and Atp6v0d1), cholesterol metabolism (Abdg5, Abcg8, Cyp7a1, and Hnf4a), and the oxidative stress response

(Gstm2, Hmox1, and Hspb1) for targeted proteomics analysis. Q Exactive HF-X mass spectrometer operating in PRM mode was employed for the analysis. Prior to PRM analysis, data-dependent acquisition (DDA) data obtained from earlier experiments were analysed via Thermo Proteome Discoverer software (version 2.4.1) to select specific peptides of the target proteins. The selected peptides were used to create the PRM method list, which included the precursor ion (m/z), charge state, and retention time window (Table S1). Based on the established method list, PRM data acquisition was performed via the Q Exactive HF-X mass spectrometer, with the MS parameters set identically to those of the previously described proteomics experiments. Quantitative analysis of the fragment ions of the target peptides in the PRM data was conducted via Skyline software (version 24.1). By analysing the peak area and signal intensity of the fragment ions, the presence and expression levels of the target proteins were confirmed.

Data processing

Untargeted metabolomic and lipidomic data processing The MS data underwent a series of pretreatment steps, such as peak picking, peak grouping, and retention time correction, via XCMS software. The raw LC-MS data files were initially converted into mzXML format and subsequently processed via XCMS, CAMERA, and the metaX toolbox [23] implemented within the R software environment. The intensity of each peak was recorded, resulting in a three-dimensional matrix comprising arbitrarily assigned peak indices (retention time-m/z pairs), sample names (observations), and ion intensity details (variables). Subsequent preprocessing of the peak intensity data was conducted via the metaX software. Features detected in less than 50% of the QC samples or 80% of the biological samples were excluded the remaining peaks with missing values were imputed with the k-nearest neighbor algorithm to further improve the data quality. Metabolome data was normalized using Probabilistic Quotient Normalization [24]. In addition, we evaluated the technical reproducibility with QC samples [25]. Low quantitative quality metabolic features mainly caused by technical error was filtered with more than 50% coefficient of variance across all QC samples [23]. To annotate the metabolites, the online Kyoto Encyclopedia of Genes and Genomes (KEGG) and Human Metabolome Databases (HMDB) were used to match the exact molecular mass data (m/z) of the samples with those in the databases. When the mass difference between the observed values and database entries was less than 10 ppm, the metabolite was annotated. For further validation of the metabolite identification, a combination of fragment databases, including Lipidblast (version 37), MassBank, HMDB (version 4.0), and an in-house fragment spectrum library was utilised.

One-way analysis of variance (ANOVA) was conducted to detect differences in metabolite and lipid concentrations among the three groups, with statistical significance determined by a p-value threshold of 0.05. To visually illustrate the differences among groups, principal component analysis (PCA) was performed via the metaX software. The variable importance in the projection (VIP) values were calculated, and a VIP threshold of 1.0 was used to select significant features. Further comparisons between the two independent sample groups were conducted via Student's t-tests. Differential metabolites were identified on the basis of a VIP > 1, a fold change (FC) > 1.5 or < 1/1.5, and an adjusted p-value (Benjamini-Hochberg) < 0.05.

Proteomic data processing The MS/MS spectra were analysed via DIA-NN (version 1.8). The analysis parameters included fixed modifications for carbamidomethylation (C), variable modifications for oxidation (M), enzyme specificity for trypsin, and a maximum of two missed cleavages. The search results were filtered to achieve a false discovery rate (FDR) of less than 1% at the protein and precursor ion levels. The remaining identifications were used for quantification.

PCA was conducted to explore the separation between groups. Subsequent comparisons between the two independent sample groups were performed via Student's t-tests. Differential proteins were identified on the basis of a fold change (FC) > 1.5 or < 1/1.5, and a p-value < 0.05.

Bioinformatics (https://www.bioinformatics.com.cn) was utilised for the visualisation of metabolomics, lipidomics, and proteomics data. The other statistical analyses were conducted using the GraphPad Prism software (version 9.5.1) in this study. One-way ANOVA was used to compare statistics, followed by Dunnett's post-hoc analysis to identify specific distinctions. The results are presented as the mean ± standard error of the mean (SEM), and statistical significance was set at $p < 0.05$.

Results

Tirzepatide alleviated the blood lipid profile and liver damage in the HFD-induced MAFLD model

To evaluate the efficacy of establishing a mouse model of fatty liver, we recorded the weekly weight changes of the mice as an indicator of model success. Compared with the NCD group, the HFD group exhibited a rapid and significant increase in body weight starting from the 6th week ($p < 0.05$) (Supplementary Fig. 1A). Furthermore, we performed ultrasound imaging on 29 mice after 20 weeks of feeding to validate the development of fatty liver. Imaging results (Supplementary Fig. 1B) indicated that in the NCD group, the kidneys were more echogenic than the liver, whereas in the HFD group, the liver

echogenicity was notably higher than that in the kidneys. This increased liver echogenicity correlated with lipid accumulation, indicating the development of fatty liver. quantified the grayscale ratio of liver parenchyma to renal cortex echo, which was recorded as the hepatorenal index (HRI). Quantification of the greyscale ratio between the hepatic parenchyma and renal cortical echoes confirmed these observations (Supplementary Fig. 1C).

To assess the effect of tirzepatide on MAFLD, we also recorded the weekly weight and food intake of the mice after tirzepatide treatment. Body weight significantly decreased in the 1st week of tirzepatide treatment, and by the 12th week, the body weight of HFD + tirzepatide group approached that of the NCD group (Fig. 1A). The weekly food intake of the HFD + tirzepatide group was significantly lower than that of the HFD group (Fig. 1B). To further verify the therapeutic effects of tirzepatide, we weighed the livers of the mice after 12 weeks of treatment. The liver weight significantly decreased in the HFD + tirzepatide group compared with the HFD group (Fig. 1C). These findings demonstrate the efficacy of tirzepatide in reducing body weight and liver fat accumulation in the HFD-induced MAFLD model.

To evaluate the effects of tirzepatide on liver damage, we measured serum levels of TG, TC, HDL-C, LDL-C, ALT and AST after 12 weeks of treatment. The levels were significantly higher in the HFD group than in the NCD group. After treatment, the TG, TC, HDL-C, and LDL-C levels were significantly decreased (Fig. 1D-G), indicating an alleviation of dyslipidaemia following the tirzepatide treatment. Tirzepatide also mitigated liver damage, as indicated by reduced serum ALT and AST levels (Fig. 1H, I).

Tirzepatide reduced hepatic steatosis and inflammation in the HFD-induced MAFLD model

Liver histology and quantification results are shown in Fig. 2A-D. HE staining and quantitative analysis revealed a significant increase in the number and volume of fat vacuoles, as well as inflammatory infiltration, in the liver tissues of HFD-fed mice. Treatment with tirzepatide notably ameliorated these histopathological changes, as evidenced by a reduction in both fat vacuoles and inflammatory infiltration (Fig. 2A, C). Furthermore, ORO staining was employed to quantify the hepatic lipid content. The results demonstrated a significant increase in lipid accumulation within the hepatocytes of the HFD group compared with those of the NCD group, with liver fat constituting approximately 50%. This pronounced lipid accumulation indicated severe fatty liver degeneration in the HFD group. However, treatment with tirzepatide significantly reduced hepatic lipid droplet deposition (Fig. 2B, D).

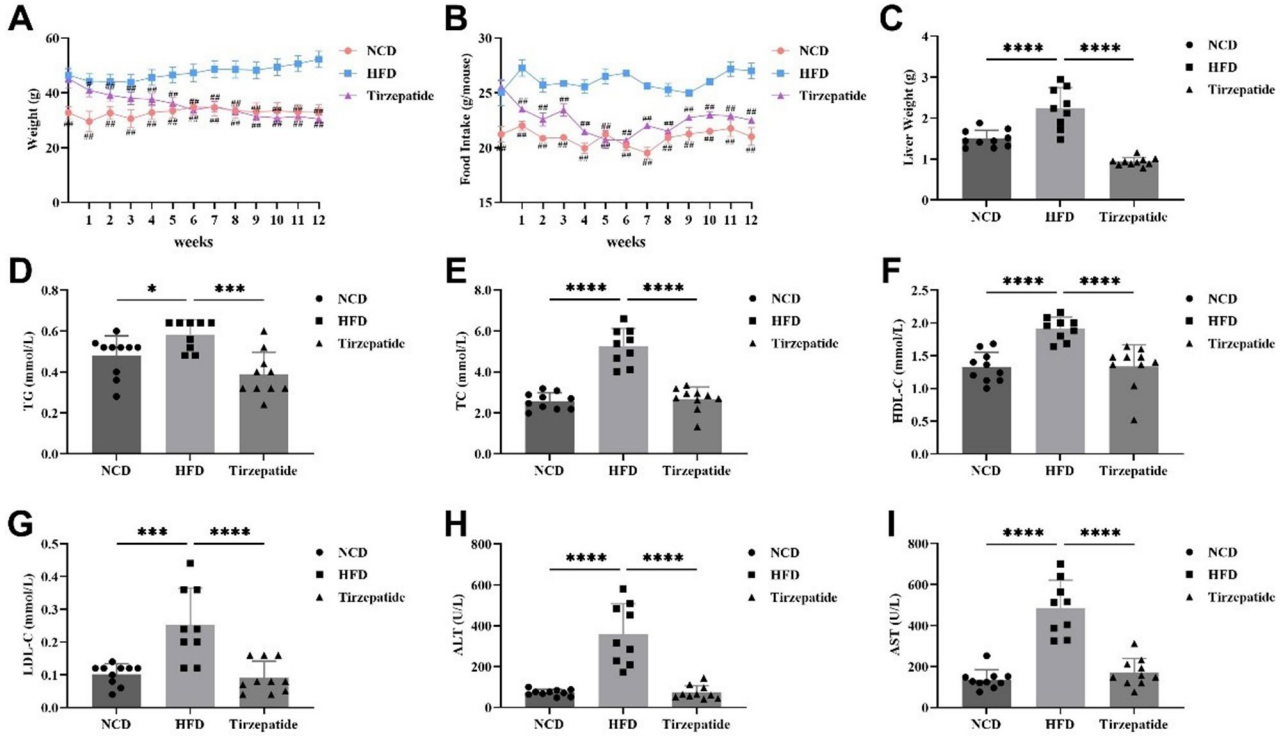

Fig. 1 Effects of tirzepatide on body weight (**A**), food intake (**B**), liver weight (**C**), serum levels of TG (**D**), TC (**E**), LDL-C (**F**), HDL-C (**G**), ALT (**H**), and AST (**I**). # $p < 0.05$, ## $p < 0.01$ compared with the HFD group. * $p < 0.05$, ** $p < 0.01$, *** $p < 0.001$, and **** $p < 0.0001$ compared with the HFD group

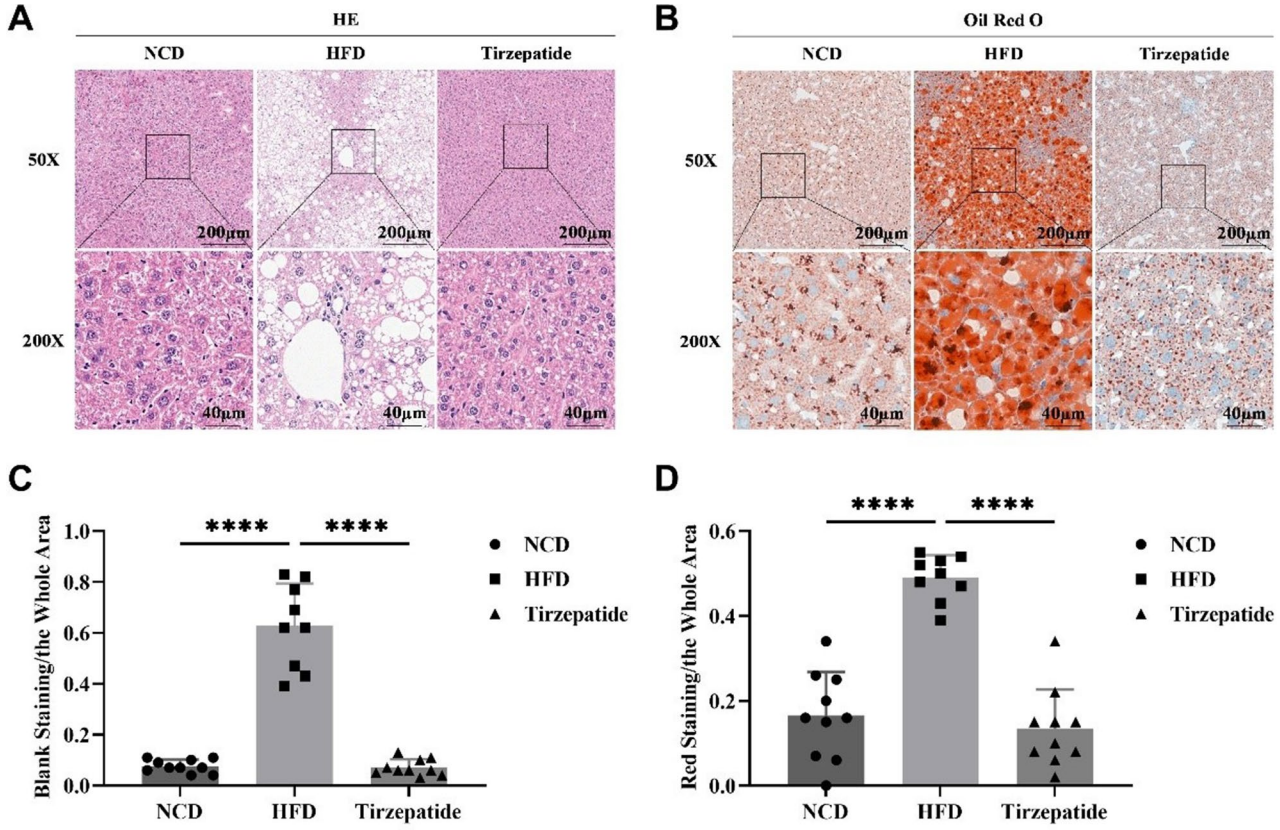

Fig. 2 Impact of tirzepatide on liver histology in the MAFLD model. Representative HE-stained liver tissue images (**A**) and representative lipid deposition images stained with ORO (**B**). Hepatic lipid accumulation was quantified as the percentage of blank (**C**) or red-stained areas (**D**) relative to the entire photomicrograph area. Significant differences were noted, with *$p < 0.05$, **$p < 0.01$, ***$p < 0.001$, and ****$p < 0.0001$ compared with the HFD group

Effects of tirzepatide on liver metabolic profiling and pathways

Using UHPLC-MS/MS in both the ESI (+) and ESI (-) modes to ensure comprehensive metabolite coverage, we identified 2,268 metabolites that were subsequently categorised into 17 superclasses across all samples (Supplementary Fig. 2A). The detected metabolites predominantly included 613 lipids and lipid-like molecules (27.03%), 521 organic acids and their derivatives (22.97%), and 334 organoheterocyclic compounds (14.73%). The separation of metabolites among the NCD, HFD, and HFD + tirzepatide groups is depicted in the PCA score plots (Fig. 3A). The results indicated that the NCD, HFD, and HFD + tirzepatide groups were distinctly separated based on their metabolic characteristics, demonstrating inter-group differences. In addition, the QC samples confirmed the reliability of the experimental procedure and the stability of the instrumentation. A total of 926 differential metabolites were identified across the three groups via one-way ANOVA. Hierarchical clustering (Supplementary Fig. 2B) and K-means clustering (Fig. 3B) analyses revealed that lipids and lipid-like molecules were significantly elevated in the HFD group compared with the NCD group. This elevation was significantly reversed following tirzepatide treatment. Similarly, organic acids and their derivatives were significantly reduced in the HFD group compared with the NCD group, and this reduction was also significantly reversed by tirzepatide treatment. These results indicate that tirzepatide may exert its therapeutic effects by modulating lipid metabolism and organic acid metabolism.

To assess the effects of tirzepatide on MAFLD metabolomics, a comparative analysis was performed between the HFD and NCD groups, and between the HFD + tirzepatide and HFD groups. The results revealed a total of 636 significant differential metabolites between the HFD and NCD groups (169 upregulated and 467 downregulated), as illustrated in the heat map (Supplementary Fig. 2C). The disrupted metabolic pathways primarily included protein digestion and absorption, glycerophospholipid metabolism, central carbon metabolism in cancer, and metabolic pathway (Fig. 3C).

In the protein digestion and absorption pathway, we observed that in the HFD group, the levels of several amino acids, including L-serine, proline, L-isoleucine, L-histidine, and L-glutamic acid, were significantly downregulated (Fig. 3D). The metabolic disruption of these amino acids may lead to abnormalities in glucose

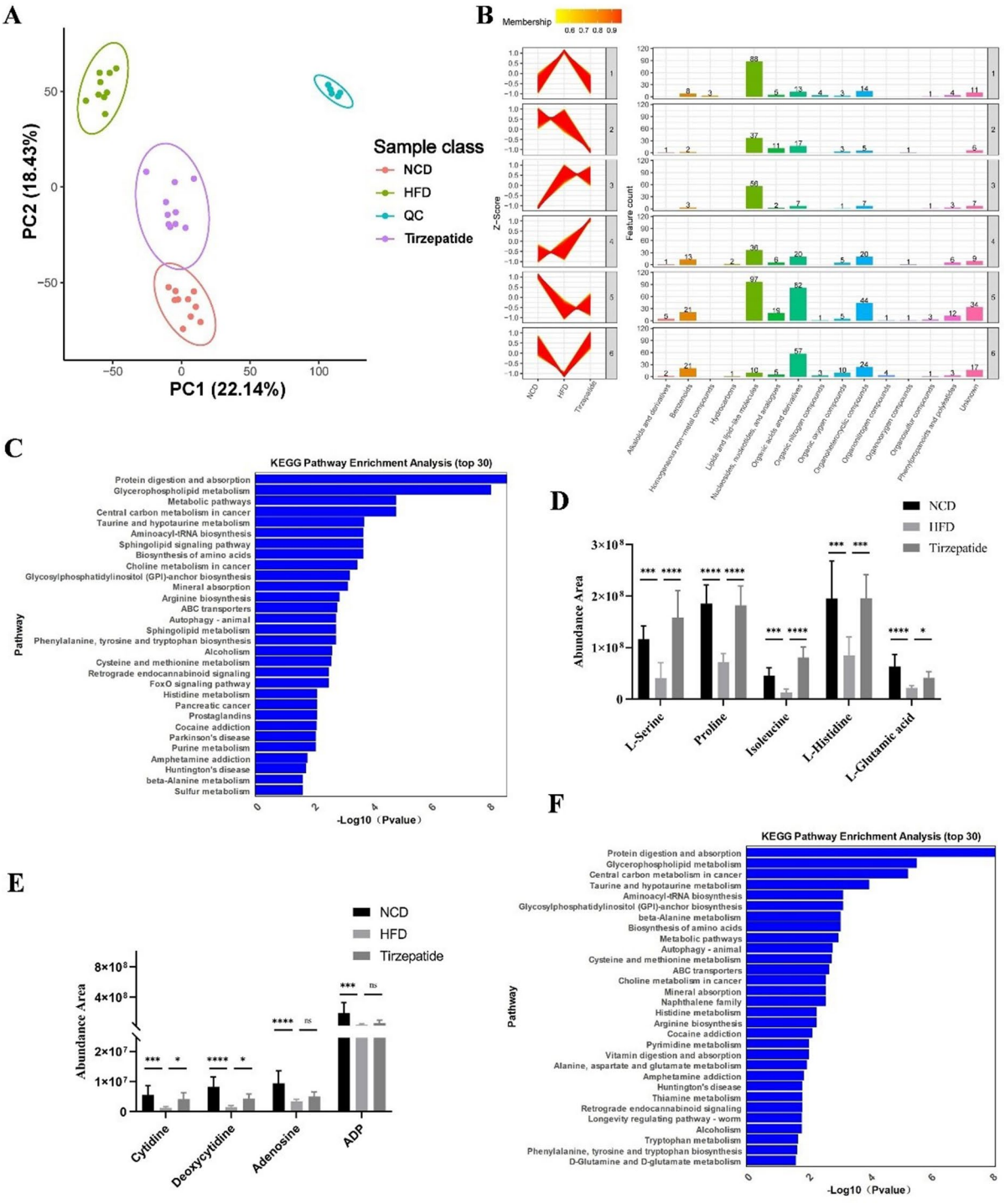

Fig. 3 Effects of tirzepatide on the liver metabolites of MAFLD mice. (**A**) PCA score plot of metabolites among the NCD, HFD, HFD + tirzepatide, and QC groups. (**B**) K-means clustering and statistical chart based on chemical taxonomy: superclass results of differential metabolites. (**C**) KEGG pathway enrichment analysis results between the HFD and NCD groups. (**D**) Effects of tirzepatide treatment on the disturbance of metabolites related to amino acids in the liver of MAFLD mice. (**E**) The contents of nucleosides, nucleotides, and their analogues in the three groups. (**F**) KEGG pathway enrichment analysis results between the HFD + tirzepatide and HFD groups

metabolism and protein synthesis. Specifically, the downregulation of L-isoleucine may result in branched-chain amino acid metabolism disorders, subsequently affecting insulin signalling and glucose metabolism [26]. Additionally, the decreased levels of L-glutamic acid and L-serine may impair glutamine synthesis [27] and one-carbon metabolism [28]. Meanwhile, in the analysis of nucleosides, nucleotides, and their analogues, we found that the levels of cytidine, deoxycytidine, adenosine, and adenosine diphosphate (ADP) tended to decrease in the HFD group (Fig. 3E). This downregulation of metabolites may be attributed to decreased amino acid levels affecting one-carbon metabolism, thereby inhibiting nucleotide synthesis pathways, which in turn impacts cellular energy metabolism and DNA/RNA synthesis.

Conversely, compared with the HFD group, after tirzepatide treatment, we identified 526 significant metabolites (377 upregulated, 149 downregulated), as shown in the heat map (Supplementary Fig. 2D). Among these, 56 metabolites were upregulated in the HFD group compared with those in the NCD group and were subsequently reduced after tirzepatide treatment. 241 metabolites were downregulated in the HFD group and then increased in the HFD + tirzepatide group. The altered metabolic pathways post-treatment mainly included protein digestion and absorption, glycerophospholipid metabolism, central carbon metabolism in cancer, as well as taurine and hypotaurine metabolism (Fig. 3F). These pathways are primarily involved in the metabolism, digestion, and absorption of proteins and lipids, highlighting the broad metabolic effects of tirzepatide treatment.

Effects of tirzepatide on liver lipidomic profiling and pathways

The analysis identified 1,378 lipid molecules through UHPLC-MS/MS in both ESI (+) and ESI (-) modes, further classified into 70 distinct lipid species (Fig. 4A). The most prevalent lipid species were 160 TG (11.61%), 136 phosphatidylcholines (PC, 9.87%), and 114 ether-linked lysophosphatidylethanolamines (Ether PE, 8.27%). A total of 772 differential lipids were identified across the three groups (NCD, HFD, and HFD + tirzepatide) via one-way ANOVA. The PCA score plot showed distinct clusters among the groups (Fig. 4B), and the clustering of QC samples indicated the stability of the experimental process. Further hierarchical clustering analysis showed significant differences in the lipid profiles among the three groups (Fig. 4C).

In addition, differential analysis was conducted between the HFD and NCD groups, as well as between the HFD + tirzepatide and HFD groups. In total, 490 significantly different lipids were identified between the HFD and NCD groups. Among these differential lipids, TG represented 12.65%, PC 12.24%, and Ether PE 9.59% (Fig. 4D). Between the HFD + tirzepatide and HFD groups, 420 differential lipids were identified, with 280 upregulated and 140 downregulated. The major differential lipids identified were TG (15.71%), Ether PE (10.71%), and PC (6.43%) (Fig. 4E). The relative contents of fatty acids (FA), phosphatidylinositol (PI), and phosphatidylglycerol (PG) were significantly upregulated in the HFD group compared to those in the NCD group. Conversely, PC, phosphatidylethanolamine (PE), and lysophophatidylcholine (LPC) levels were downregulated. In the HFD group, the profiles of Triglycerides (TG, 66.13%) and diacylglycerol (DG, 26.67%) were upregulated (Supplementary Fig. 3A). In the HFD + tirzepatide group, the relative levels of PC, PE, and LPC were significantly upregulated compared with those in the HFD group, whereas the levels of DG, PI, and FA were downregulated. Furthermore, the TG levels (65.15%) were also decreased (Supplementary Fig. 3B). These results indicated that tirzepatide treatment induced a notable shift in circulating lipid profiles, suggesting potential therapeutic effects on lipid metabolism in MAFLD.

Identification of key protein targets and potential mechanisms of tirzepatide

A total of 6838 quantifiable proteins were identified via LC-MS/MS. Visualisation of protein separation between the HFD and NCD groups, as well as the HFD + tirzepatide and HFD groups, was accomplished using PCA score plots (Fig. 5A, B). The plot showed that the protein profiles were distinctly segregated, indicating considerable variability, primarily through two principal components.

The study identified 753 differentially regulated proteins (356 upregulated and 397 downregulated) in the HFD group compared with the NCD group (Supplementary Fig. 4A), and 794 differentially regulated proteins (511 upregulated and 283 downregulated) in the HFD group compared with the HFD group (Supplementary Fig. 4B). Among these, 162 upregulated proteins in the HFD group were modulated by tirzepatide treatment and 201 downregulated proteins in the HFD group were restored to normal levels by tirzepatide treatment (Supplementary Fig. 4C).

To further understand the biological functions and key pathways involved in tirzepatide treatment for MAFLD, we conducted functional enrichment analysis via Gene Ontology (GO) and KEGG. Compared with the NCD group, the HFD group exhibited significant changes in biological processes (BP) such as cellular lipid metabolism and fatty acid metabolic. In the cellular component (CC) category, enrichment analysis revealed significant alterations in peroxisome and autophagosome membrane. Molecular function (MF) analysis indicated significant changes in oxidoreductase activity and catalytic

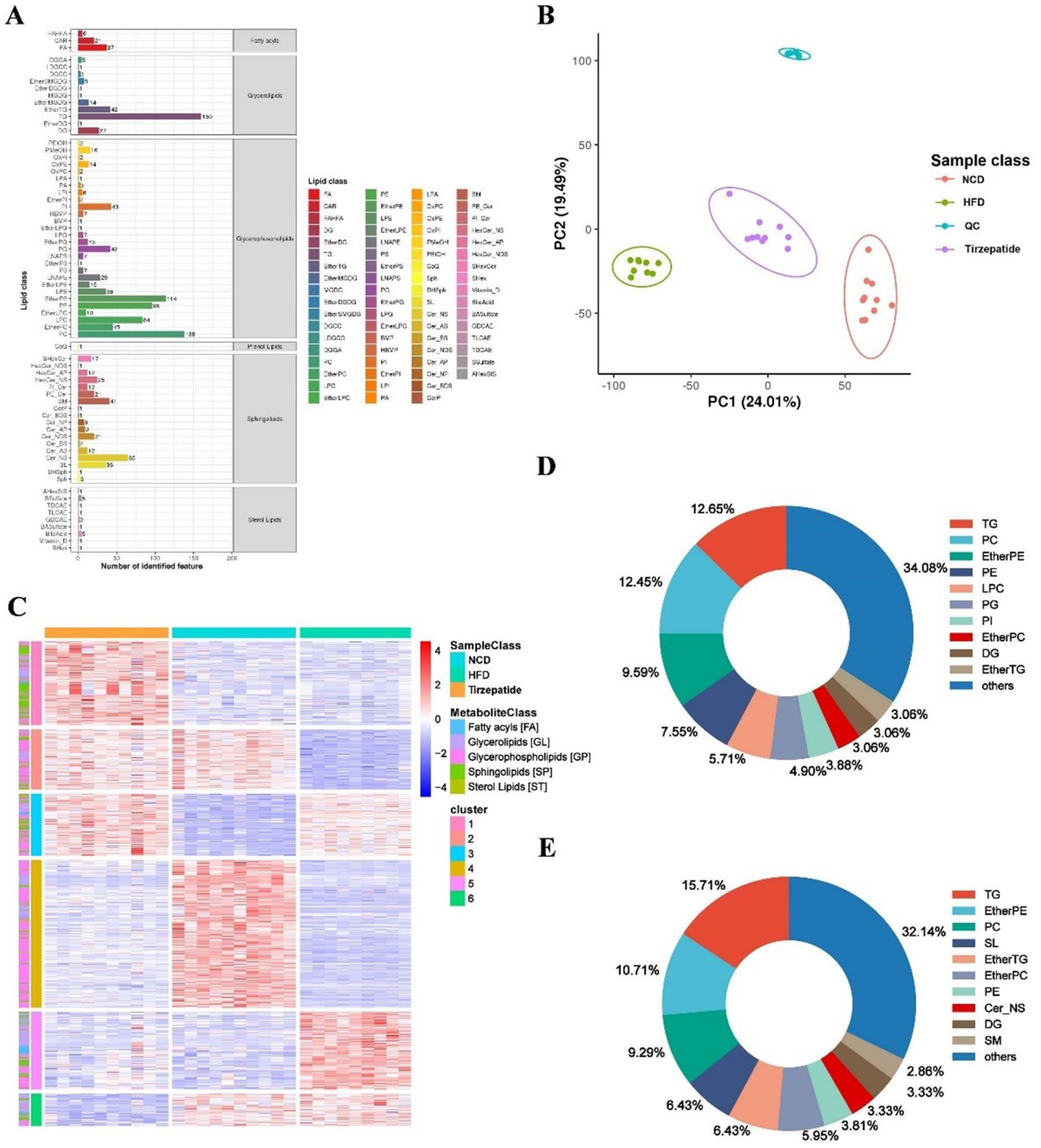

Fig. 4 Effects of tirzepatide on the liver lipids of mice with MAFLD. (**A**) Statistical chart of lipid classes. (**B**) PCA score plot of lipids among the NCD, HFD, HFD + tirzepatide, and QC groups. (**C**) Heatmap of hierarchical clustering analysis for differential lipids of the NCD, HFD, and HFD + tirzepatide groups. Pie charts showing the lipid classes of differentially expressed lipids between the HFD and NCD groups (**D**), and between the HFD + tirzepatide and HFD groups (**E**)

activity (Fig. 5C). KEGG pathway enrichment analysis further revealed that the differential proteins were primarily involved in key pathways such as retinol metabolism, steroid hormone biosynthesis, PPAR signalling pathway, lysosome, and fatty acid degradation, all of which are closely related to lipid metabolism and protein degradation (Fig. 5D).

In the PPAR signalling pathway, the expression of FA transport proteins (Cd36), fatty acid-binding proteins (Fabp2, Fabp4), and perilipins (Plin2, Plin4, and Plin5)

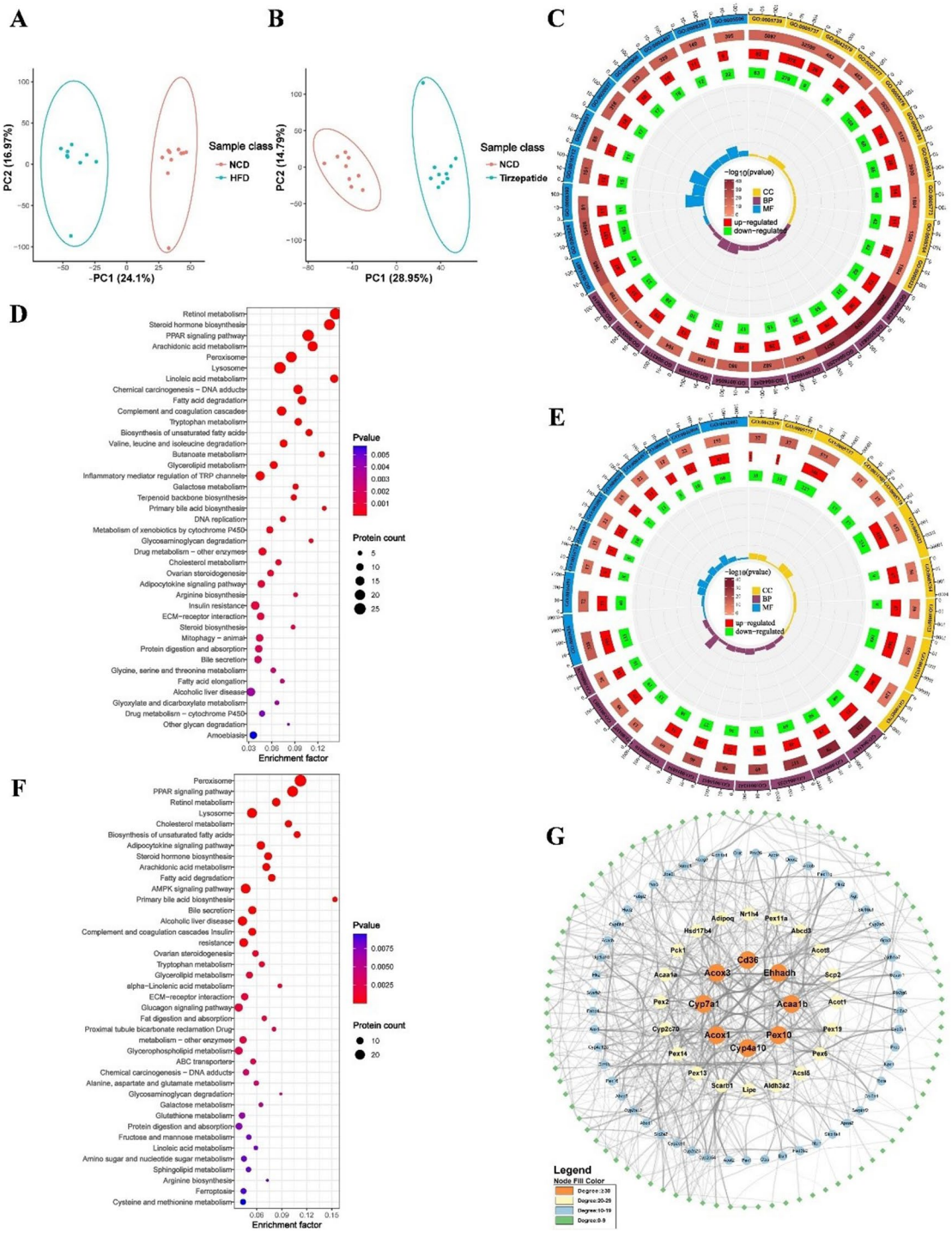

Fig. 5 Effects of tirzepatide on the liver proteins in MAFLD mice. PCA score plot of proteins between the HFD and NCD groups (**A**), and between the HFD + tirzepatide and HFD groups (**B**). (**C**) GO enrichment analysis of differentially expressed proteins between the HFD and NCD groups. (**D**) KEGG pathway enrichment analysis of differentially expressed proteins between the HFD and NCD groups. (**E**) GO enrichment analysis of differentially expressed proteins between the HFD + tirzepatide and HFD groups. (**F**) KEGG pathway enrichment analysis of differentially expressed proteins between the HFD + tirzepatide and HFD groups. (**G**) PPI network of differentially expressed proteins between the HFD + tirzepatide and HFD groups

associated with lipid accumulation were significantly increased. This was consistent with the lipidomic results showing increased FA and TG in the HFD group. Furthermore, the upregulation of FAO related proteins such as Cpt1a, Acaa1b, Ehhadh, and Cyp4a10 suggests that the liver is attempting to counteract lipid accumulation by increasing FAO.

Additional differential enrichment analysis found that proteins related to the mitophagy pathway, such as Sqstm1, Bnip3, Map1lc3b, and Optn, were significantly upregulated, suggesting an increase in mitochondrial damage. However, in the lysosomal pathway, most acid hydrolases and Atp6v0d1 were downregulated. The downregulation of Atp6v0d1 indicates a potential reduction in the conversion of ATP to ADP, which may affect the pH of lysosomes. Metabolomics data also showed decreased ADP levels, further supporting the hypothesis of altered lysosomal pH.

Compared to the HFD group, tirzepatide treatment exhibited significant changes in various BP, particularly in cellular lipid catabolic and peroxisomal transport. In the CC category, enrichment analysis revealed significant changes in the microbody membrane and peroxisomal membrane, suggesting the critical role of these membrane structures in metabolic regulation. MF analysis indicated that tirzepatide treatment significantly regulated steroid hydroxylase activity and acyl-CoA hydrolase activity. These changes in enzyme activity may directly impact lipid metabolic pathways (Fig. 5E).

KEGG pathway enrichment analysis indicated that the differential proteins following tirzepatide treatment were primarily enriched in key metabolic pathways such as PPAR signalling pathway, lysosome, cholesterol metabolism, retinol metabolism, and fatty acid degradation (Fig. 5F). Within the cholesterol metabolism pathway, we observed a significant upregulation of Abcg5 and Abcg8 after tirzepatide treatment. Furthermore, the protein Hnf4a, a regulator of cholesterol metabolism, was markedly upregulated. These findings suggest that post-treatment, there was an increased transport of cholesterol to the gallbladder, potentially reducing cholesterol accumulation. Thus, these findings imply that tirzepatide may reduce lipid accumulation and protect hepatocytes through multiple mechanisms.

In addition, we employed the STRING database to perform a protein-protein interaction (PPI) network analyses on 188 proteins enriched in significant KEGG pathways ($p < 0.05$) between the HFD group and the HFD + tirzepatide group. Subsequently, we visualised the network using Cytoscape software (Fig. 5G). This analysis showed that several critical proteins, including Cyp7a1, Scarb1, Pck1, Abcg5, Abcg8, and Nr1h4 were significantly upregulated after post-treatment, indicating enhanced liver function and bile acid metabolism. In contrast, proteins such as CD36, Acox3, Acaa1b, Ehhadh, Cyp4a10, Hsd17b4, Adipoq, and Lipe were significantly downregulated, suggesting reduced lipid peroxidation and inflammation. These proteins are known for their substantial roles in liver metabolism, lipid transport, and the inflammatory response.

Integration analysis of the mechanistic effects of tirzepatide in MAFLD

To further investigate the molecular mechanisms through which tirzepatide alleviates MAFLD, we conducted a comprehensive analysis of liver tissues via metabolomics, lipidomics, and proteomics. Our findings indicate that tirzepatide treatment reverses the key disrupted metabolic and mitophagic pathways identified in MAFLD mice, as shown in Fig. 6. After treatment with tirzepatide, the expression of free fatty acids (FFA) and FA transport proteins (Fabp2, Fabp5, and Cd36) was significantly downregulated, potentially reducing hepatic lipid uptake. In addition, the levels of DG, TG, and lipid droplet proteins (Plin2, Plin4, and Plin5) were significantly reduced, which was consistent with the observed decrease in hepatic lipid accumulation. Further analysis revealed that key proteins involved in gluconeogenesis, pentose phosphate pathway, and glycogen synthesis were significantly upregulated after administration, indicating the restoration of glucose metabolism. FA oxidation-associated proteins (Ehhadh, Acaa1a, Acaa1b, and Cyp4a10) were downregulated after tirzepatide treatment, suggesting a reduction in compensatory lipid oxidation. This may have a positive effect on alleviating oxidative stress and protecting the mitochondria from damage. Furthermore, the lysosome-related compounds D-mannose-6-phosphate (M6P) and Tcirg1 protein were upregulated ($p < 0.05$), ensuring proper transport and activity of lysosomal acid hydrolases. Concurrently, the metabolic disturbances in phospholipids (PC, PI, PG, and PS), amino acids, cholesterol, and bile acids were corrected ($p < 0.05$) following tirzepatide treatment. In summary, tirzepatide alleviates MAFLD pathology through multiple pathways, including the improvement of cholesterol, glucose, and lipid metabolism, as well as the enhancement of mitophagy.

Validation of multiple mechanisms of tirzepatide treatment in MAFLD mice

To further elucidate the molecular mechanisms by which tirzepatide treats MAFLD in mice, we conducted PRM experiments on liver tissues to verify the reliability of protein expression levels.

In the HFD group, the expression levels of Cd36, Fabp2, Fabp4, Plin2, Plin4, and Plin5 were significantly upregulated. After tirzepatide treatment, the expression of these proteins was significantly reduced (Fig. 7A). FAO-related proteins Cpt1a, Acaa1b, and Cyp4a10 were significantly

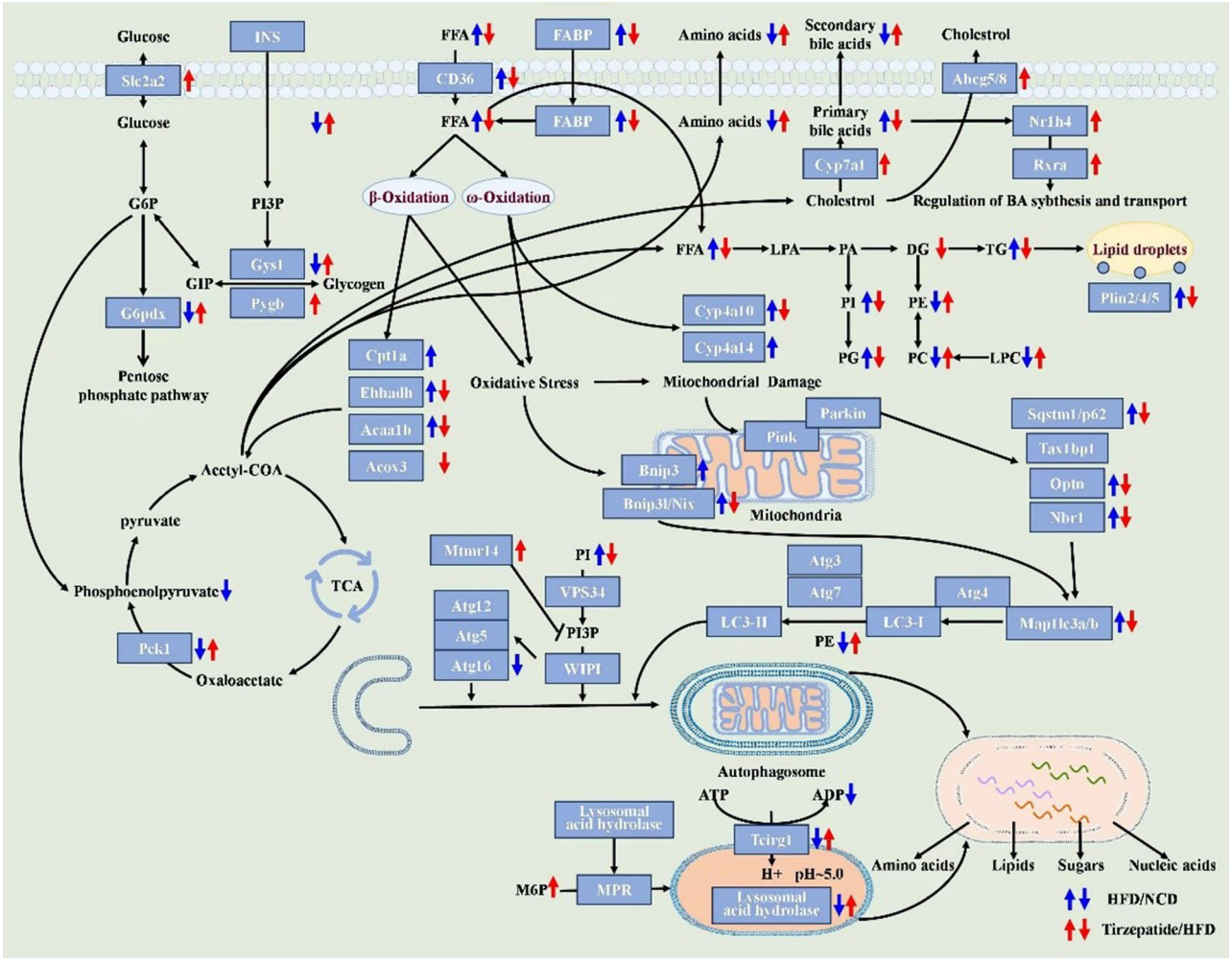

Fig. 6 Tirzepatide reverses key disrupted metabolic and mitophagic pathways in mice with MAFLD

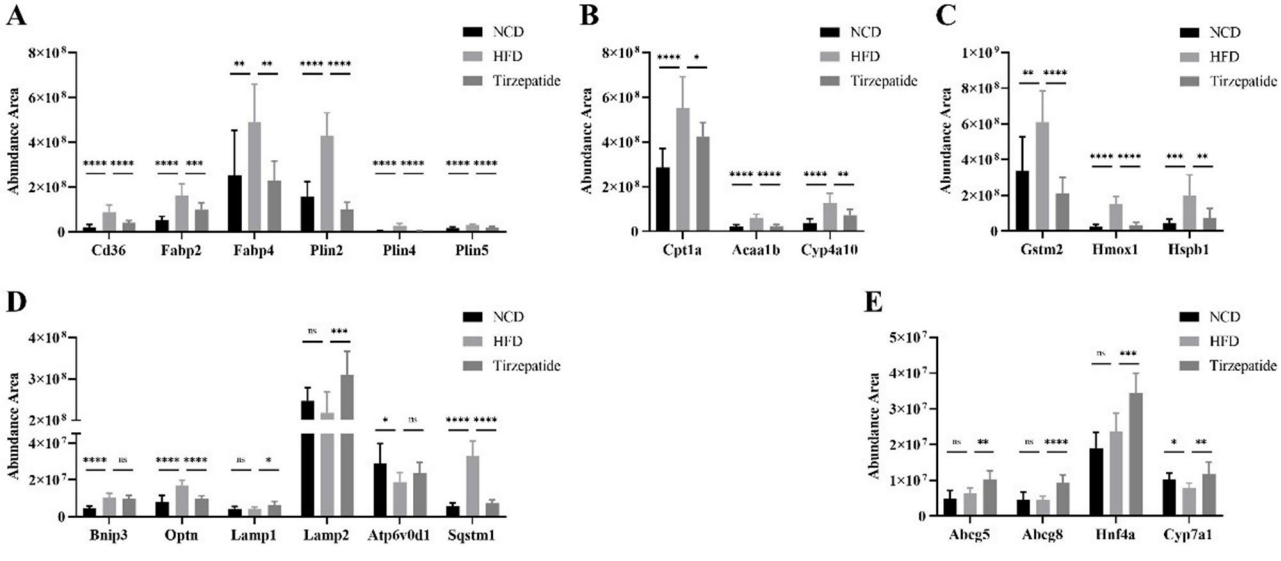

Fig. 7 Validation of protein expression levels using PRM in liver tissues of mice. The contents of proteins related to lipid synthesis (Cd36, Fabp2, Fabp4, Plin2, Plin4, and Plin5) (**A**), FAO (Cpt1a, Acaa1b, and Cyp4a10) (**B**), oxidative stress response (Gstm2, Hmox1, and Hspb1) (**C**), mitophagy-lysosome pathway (Bnip3, Sqstm1, Optn, Lamp1, Lamp2, and Atp6v0d1) (**D**), and cholesterol metabolism (Abdg5, Abcg8, Cyp7a1, and Hnf4a) (**E**) in three groups

upregulated in the HFD group (Fig. 7B), along with antioxidant stress proteins Gstm2, Hmox1, and Hspb1. In the tirzepatide treatment group, the expression of these proteins was significantly reduced, suggesting that tirzepatide can alleviate oxidative stress (Fig. 7C). Mitochondrial autophagy-related proteins (Bnip3 and Optn) were significantly elevated in the HFD group, while lysosome-related protein Atp6v0d1 was significantly downregulated. After tirzepatide treatment, mitochondrial autophagy-related protein Optn was downregulated, and lysosome-related proteins (Lamp1 and Lamp2) were upregulated (Fig. 7D). Additionally, we found that proteins involved in cholesterol metabolism, such as Abcg5, Abcg8, Cyp7a1, and Hnf4a, were significantly upregulated after tirzepatide treatment (Fig. 7E), which increased the direct transport of cholesterol to the gallbladder and its excretion via faeces, thereby reducing the amount of cholesterol in systemic circulation.

Discussion

MAFLD is significantly influenced by unbalanced dietary habits, such as high-fat and high-sugar intake [29, 30]. Our study demonstrated that the HFD mouse model exhibits notable hepatic fat accumulation, which increases the risk of MAFLD. MAFLD is strongly associated with the development of NASH, liver cirrhosis, hepatocellular carcinoma [31], along with cardiovascular diseases [32] and type 2 diabetes [33]. Although lifestyle modifications such as dietary management and physical activity can enhance MAFLD outcomes, sustaining these alterations over extended periods is often difficult for individuals. Presently, no medication has gained widespread approval for MAFLD therapy; however, certain pharmaceuticals have demonstrated potential in clinical trials [34–36].

Our results indicated that tirzepatide significantly decreased liver damage and lipid metabolism disruption in MAFLD mice ($p < 0.05$), as evidenced by a decrease in body weight and serum concentrations of ALT, AST, TC, TG, and LDL-C ($p < 0.05$). Histopathological evaluations revealed a reduction in hepatic lipid accumulation, consistent with previous research suggesting the potential of tirzepatide for the therapeutic treatment of fatty liver [37, 38].

Individual GLP-1R [39, 40] or GIPR [41] agonists may exert their effects through the central nervous system, stimulating receptors on neurones that regulate appetite to decrease food consumption and appetite, and enhance satiety. Recent studies have indicated that GIPR/GLP1R agonists stimulate these neurones more potently than single agonists, resulting in substantial reductions in food intake and body weight [15, 38, 42]. This, at least partly, accounts for the additional decrease in hepatic steatosis observed with tirzepatide treatment, likely by diminishing the flow of nutrients to the liver.

Through comprehensive metabolomics, lipidomics, and proteomics analyses, we identified that the PPAR pathway plays a crucial role in lipid metabolism regulation and the progression of MAFLD. Specifically, in comparison with the NCD group, the expression of proteins associated with PPAR pathway activation was markedly elevated in the HFD group, including Cd36, Fabp2, Fabp4, Plin2, Plin4, Plin5, Capt1a, Acaa1b, and Cyp4a10 ($p < 0.05$) [43]. Reports have shown that the upregulation of Cd36 contributes to lipid accumulation and triggers inflammatory responses through the activation of the JNK pathway [44]. Cd36 is a key protein involved in the uptake of free FFA by the liver. Increased Cd36 expression suggests enhanced hepatic uptake of FFAs, indicating an increased influx of lipids. Fabp2 and Fabp4 are fatty acid-binding proteins that facilitate intracellular transport of these FA, further explaining the elevated levels of FFAs such as palmitelaidic acid, palmitic acid, oleic acid, and cis-8,11,14,17-eicosatetraenoic acid in the liver. In addition, the significant upregulation of Plin2, Plin4, and Plin5 in the HFD group, which are lipid droplet-associated proteins, promotes steatosis. Hepatic lipidomic results revealed elevated levels of TG, PI, and PG, indicating significant lipid accumulation. Proteins involved in FAO, such as the FA β-oxidation proteins Capt1a and Acaa1b and the FA ω-oxidation protein Cyp4a10, were significantly increased in the HFD group, suggesting that the liver attempts to reduce lipid accumulation by enhancing FAO. However, this compensatory increase in FAO can lead to mitochondrial overloading and subsequent damage, resulting in increased oxidative stress and inflammatory responses [45, 46].

We also found a significant increase in the expression of proteins related to antioxidative stress, such as Gstm2, Hspb1, and Hmox1, in the HFD group ($p < 0.05$), further confirming that the compensatory increase in FAO may stimulate oxidative stress and inflammation regulation [47, 48]. In conclusion, our findings suggest that while the activation of the PPAR pathway helps reduce lipid accumulation and inflammatory responses, the compensatory upregulation of FAO may exacerbate oxidative stress and inflammation by overproducing reactive oxygen species (ROS) [49].

Post-treatment with tirzepatide, resulted in a significant reduction in the levels of key proteins and metabolites ($p < 0.05$). This suggests that tirzepatide may alleviate oxidative stress and inflammation by downregulating proteins involved in lipid synthesis and FAO, thereby reducing overall FAO and ROS production.

The PRM results also revealed that the concentrations of proteins involved in mitophagy, such as Bnip3 and Optn, were significantly higher in the high-fat diet (HFD)

group compared to the NCD group ($p < 0.05$), indicating enhanced mitophagy [50]. Increased mitophagy is typically associated with elevated mitochondrial damage, which aids in the clearance of dysfunctional mitochondria and maintains cellular stability. Given the close connection between mitochondrial damage and oxidative stress [51, 52], the elevation of mitophagy could also indicate an escalation in the internal oxidative stress levels within the liver. Mitophagy, a vital aspect of autophagy, is an essential degradation and recycling mechanism within cells. After autophagosome formation, fusion with lysosomes forms autolysosomes, where lysosomal hydrolases degrade the enclosed material and recycle small molecules, such as amino acids and nucleotides [53]. The fusion of autophagosomes and lysosomes is mediated by Snare proteins [53]. In our study, we detected a significant downregulation of the key lipid PE, which promotes the interaction between Snare and LC3-I, indicating impaired fusion of autophagosomes and lysosomes [54]. Moreover, the results demonstrated a significant upregulation of Sqstm1 (P62, which is inversely related to autophagic activity) protein in the HFD group, suggesting that the autophagic process might be hindered [55]. The accumulation of P62 protein generally reflects a blockage in autophagic flux, meaning that autophagosomes cannot effectively fuse with lysosomes for degradation. Recent reports [56] have shown that Cd36 can recruit Ubqln1 to promote Snare protein degradation, providing further evidence for the inhibition of autophagosome-lysosome fusion.

In addition, enrichment analysis indicated disruptions in the lysosomal pathway within the HFD group, where the expression levels of some acidic hydrolases were decreased. Atp6v0d1, which converts ATP to ADP, was significantly downregulated ($p < 0.05$), affecting the pH balance within lysosomes [57]. Metabolomic data revealed a significant downregulation in the expression of ADP, amino acids (such as L-serine, proline, L-isoleucine, L-histidine, and L-glutamic acid), as well as nucleosides, nucleotides, and their analogues (including Cytidine, Deoxycytidine, and Adenosine). These findings further suggest defects in autolysosomal function. Post-treatment with tirzepatide led to a downregulation of Optn expression level, potentially indicating reduced mitochondrial damage. Concurrently, there was a significant upregulation in Lamp1 and Lamp2 (Proteins involved in the regulation of lysosomal pH) [58], lysosomal acidic hydrolases, and metabolites such as PE and M6P (a signalling molecule for the transportation of newly synthesised lysosomal enzymes to lysosomes) [59], while Sqstm1 protein levels were notably downregulated. This indicates that the drug may enhance lysosomal function and facilitate the fusion of autophagosomes and lysosomes, thereby restoring normal lipid and protein degradation and autophagic function. This may indicate the capacity of the drug to enhance lysosomal function recovery and the fusion of autophagosomes and lysosomes, thereby facilitating the normal degradation of lipids and proteins and restoration of autophagic function.

Furthermore, we observed significant changes in cholesterol metabolism following tirzepatide administration, as indicated by the proteomics and metabolomics results ($p < 0.05$). Metabolomics data showed that, compared to the NCD group, the HFD group exhibited a significant increase in the expression of primary bile acids (cholic acid) and their conjugated form (taurocholic acid), as well as the bile acid-sensing nuclear receptor Nr1h4 antagonist (tauro-β-muricholic acid) ($p < 0.05$) [60]. Conversely, the expression of Cyp7a1, the key enzyme responsible for converting cholesterol into bile acids, was significantly downregulated ($p < 0.05$). The downregulation of Cyp7a1, crucial for cholesterol to bile acid conversion, resulted in a reduced efficiency of this process and subsequent cholesterol accumulation in the liver. Reports [61] indicate that heightened expression of Cd36 enhances chronic inflammatory signalling, reduces cholesterol excretion, leads to hepatic cholesterol accumulation, and contributes to fatty liver disease. This suggests a potential disruption in cholesterol-bile acid metabolism, where cholesterol accumulation and reduced bile acid synthesis may trigger inflammatory responses and hepatocyte damage [62]. In the HFD + tirzepatide group, the expression of the cholesterol transporter Abcg5 and Abcg8 was significantly increased ($p < 0.05$), thereby enhancing cholesterol efflux capacity [63]. The upregulation of Hnf4a, Abcg5, and Abcg8 was accompanied by a significant decrease in taurocholic acid levels. The upregulation of Hnf4a not only optimised bile acid metabolism directly but also promoted the expressions of Abcg5 and Abcg8 by regulating related genes. These findings suggest that tirzepatide significantly improves cholesterol and bile acid metabolism and excretion by upregulating key transporters and nuclear receptors, thereby alleviating the pathological state of fatty liver disease.

Conclusion

Our study provides evidence for the potential of tirzepatide to alleviate lipid accumulation and maintain hepatocyte function in the HFD mouse model, underscoring its application prospects in treating metabolic diseases. By integrating metabolomics, lipidomics, and proteomics analyses, combined with PRM validation, we identified that tirzepatide exerts its effects through multiple mechanisms. These mechanisms include reducing FA uptake and lipid accumulation, enhancing mitochondria-lysosome function, improving lipid metabolism, and regulating cholesterol metabolism. Collectively, these effects

significantly ameliorate the pathological state of fatty liver.

Abbreviations

MAFLD	Metabolic dysfunction-associated fatty liver disease
MASH	Metabolic dysfunction-associated steatohepatitis
LC-MS	Liquid chromatography-mass spectrometry
UPLC-Orbitrap-MS/MS	Ultra-performance liquid chromatography coupled with Orbitrap tandem mass spectrometry
ALT	Alanine transaminase
AST	Aspartate transaminase
TG	Triglycerides
TC	Total cholesterol
HDL-C	high-density lipoprotein cholesterol
LDL-C	Low-density lipoprotein cholesterol
HFD	High-fat diet
NCD	Normal diet group
GLP-1	Glucagon-like peptide-1
GIP	Glucose-dependent insulinotropic polypeptide
HE	Haematoxylin and eosin
ORO	Oil Red O
HRI	hepatorenal index
DIA	Data-independent acquisition
DDA	Data-dependent acquisition
PRM	Parallel reaction monitoring
PPI	Protein-protein interaction
M6P	D-mannose-6-phosphate

Supplementary Information

The online version contains supplementary material available at https://doi.org/10.1186/s12944-024-02416-2.

Supplementary Material 1

Acknowledgements

We thank Baojin Zhou from Deepxomics Co., Ltd. for his technical support in omics.

Author contributions

Jinliang Liang: Methodology, Investigation, Writing – original draft, Writing – review and editing. Huanyi Liu: Methodology, Investigation, Data curation. Guo Lv: Methodology, Investigation. Xiaotong Chen: Methodology, Zhaoshou Yang: Methodology. Kunhua Hu: Writing – original draft, Writing – review and editing. Hongyan Sun: Methodology, Data curation, Writing – original draft, Writing – review and editing.

Funding

This work was supported by the National Natural Science Foundation of China (82472868 and 82172585), the Science and Technology Projects in Guangzhou (2024A03J0101 and 202103000051), the Science and Technology Program of Guangdong (2020B1212060019).

Data availability

The original omics data used in the current study are publicly available at the National Genomics Data Center (NGDC). They can be accessed via the following link: https://ngdc.cncb.ac.cn/omix/, under the accession numbers OMIX007944, OMIX007945 and OMIX007946.

Declarations

Ethics approval and consent to participate

All animal experiments were approved by the Institutional Animal Care and Use Committee of Guangzhou Jennio Biotechnology Co., Ltd. (Approval No. JENNIO-IACUC-2023-A066).

Consent for publication

Not applicable.

Competing interests

The authors declare no competing interests.

Received: 16 October 2024 / Accepted: 19 December 2024
Published online: 10 January 2025

References

1. Riazi K, Azhari H, Charette JH, et al. The prevalence and incidence of NAFLD worldwide: a systematic review and meta-analysis. Lancet Gastroenterol Hepatol. 2022;7(9):851–61. https://doi.org/10.1016/s2468-1253(22)00165-0.
2. Powell EE, Wong VW-S, Rinella M. Non-alcoholic fatty liver disease. Lancet. 2021;397(10290):2212–24. https://doi.org/10.1016/s0140-6736(20)32511-3.
3. Li H-Y, Huang S-Y, Zhou D-D, et al. Theabrownin inhibits obesity and non-alcoholic fatty liver disease in mice via serotonin-related signaling pathways and gut-liver axis. J Adv Res. 2023;52:59–72. https://doi.org/10.1016/j.jare.2023.01.008.
4. Harrison SA, Allen AM, Dubourg J, et al. Challenges and opportunities in NASH drug development. Nat Med. 2023;29(3):562–73. https://doi.org/10.1038/s41591-023-02242-6.
5. Verschuren L, Mak AL, van Koppen A, et al. Development of a novel non-invasive biomarker panel for hepatic fibrosis in MASLD. Nat Commun. 2024;15(1):4564. https://doi.org/10.1038/s41467-024-48956-0.
6. Targher G, Byrne CD, Tilg H. NAFLD and increased risk of cardiovascular disease: clinical associations, pathophysiological mechanisms and pharmacological implications. Gut. 2020;69(9):1691–705. https://doi.org/10.1136/gutjnl-2020-320622.
7. Targher G, Tilg H, Byrne CD. Non-alcoholic fatty liver disease: a multisystem disease requiring a multidisciplinary and holistic approach, the lancet. Gastroenterol Hepatol. 2021;6(7):578–88. https://doi.org/10.1016/s2468-1253(21)00020-0.
8. Hammoud R, Drucker. Beyond the pancreas: contrasting cardiometabolic actions of GIP and GLP1, Nature reviews. Endocrinology. 2023;19(4):201–16. https://doi.org/10.1038/s41574-022-00783-3.
9. Ding X, Saxena NK, Lin S, et al. Exendin-4, a glucagon-like protein-1 (GLP-1) receptor agonist, reverses hepatic steatosis in ob/ob mice. Hepatology (Baltimore MD). 2006;43(1):173–81. https://doi.org/10.1002/hep.21006.
10. Drucker DJ. Mechanisms of action and therapeutic application of glucagon-like Peptide-1. Cell Metabol. 2018;27(4):740–56. https://doi.org/10.1016/j.cmet.2018.03.001.
11. Adriaenssens AE, Biggs EK, Darwish T, et al. Glucose-dependent insulinotropic polypeptide receptor-expressing cells in the Hypothalamus regulate Food Intake. Cell Metabol. 2019;30(5):987–e996986. https://doi.org/10.1016/j.cmet.2019.07.013.
12. Zhang Q, Delessa CT, Augustin R, et al. The glucose-dependent insulinotropic polypeptide (GIP) regulates body weight and food intake via CNS-GIPR signaling. Cell Metabol. 2021;33(4):833–e844835. https://doi.org/10.1016/j.cmet.2021.01.015.
13. Weghuber D, Barrett T, Barrientos-Pérez M, et al. Once-weekly semaglutide in adolescents with obesity. N Engl J Med. 2022;387(24):2245–57. https://doi.org/10.1056/NEJMoa2208601.
14. Syed YY. Tirzepatide: First Approval Drugs. 2022;82(11):1213–20. https://doi.org/10.1007/s40265-022-01746-8.
15. Samms RJ, Coghlan MP, Sloop KW. How may GIP enhance the therapeutic efficacy of GLP-1? Trends in endocrinology and metabolism. TEM. 2020;31(6):410–21. https://doi.org/10.1016/j.tem.2020.02.006.
16. El K, Douros JD, Willard FS, et al. The incretin co-agonist tirzepatide requires GIPR for hormone secretion from human islets. Nat Metabolism. 2023;5(6):945–54. https://doi.org/10.1038/s42255-023-00811-0.
17. Samms RJ, Christe ME, Collins KA, et al. GIPR agonism mediates weight-independent insulin sensitization by tirzepatide in obese mice. J Clin Investig. 2021;131(12). https://doi.org/10.1172/jci146353.
18. Wadden TA, Chao AM, Machineni S, et al. Tirzepatide after intensive lifestyle intervention in adults with overweight or obesity: the SURMOUNT-3 phase 3 trial. Nat Med. 2023;29(11):2909–18. https://doi.org/10.1038/s41591-023-02597-w.
19. Jastreboff AM, Aronne LJ, Ahmad NN, et al. Tirzepatide once Weekly for the treatment of obesity. N Engl J Med. 2022;387(3):205–16. https://doi.org/10.1056/NEJMoa2206038.
20. Guo X, Lei M, Zhao J, et al. Tirzepatide ameliorates spatial learning and memory impairment through modulation of aberrant insulin resistance and

inflammation response in diabetic rats. Front Pharmacol. 2023;14:1146960. https://doi.org/10.3389/fphar.2023.1146960.
21. Targher G, Mantovani A, Byrne CD. Mechanisms and possible hepatoprotective effects of glucagon-like peptide-1 receptor agonists and other incretin receptor agonists in non-alcoholic fatty liver disease, the lancet. Gastroenterol Hepatol. 2023;8(2):179–91. https://doi.org/10.1016/s2468-1253(22)00338-7.
22. Hasin Y, Seldin M, Lusis A. Multi-omics approaches to disease. Genome Biol. 2017;18(1):83. https://doi.org/10.1186/s13059-017-1215-1.
23. Wen B, Mei Z, Zeng C, et al. metaX: a flexible and comprehensive software for processing metabolomics data. BMC Bioinformatics. 2017;18(1):183. https://doi.org/10.1186/s12859-017-1579-y.
24. Dieterle F, Ross A, Schlotterbeck G, et al. Probabilistic quotient normalization as robust method to account for dilution of complex biological mixtures. Application in 1H NMR metabonomics. Anal Chem. 2006;78(13):4281–90. https://doi.org/10.1021/ac051632c.
25. Dunn WB, Broadhurst D, Begley P, et al. Procedures for large-scale metabolic profiling of serum and plasma using gas chromatography and liquid chromatography coupled to mass spectrometry. Nat Protoc. 2011;6(7):1060–83. https://doi.org/10.1038/nprot.2011.335.
26. White PJ, McGarrah RW, Grimsrud PA, et al. The BCKDH kinase and Phosphatase Integrate BCAA and lipid metabolism via regulation of ATP-Citrate lyase. Cell Metabol. 2018;27(6):1281–e12931287. https://doi.org/10.1016/j.cmet.2018.04.015.
27. Eelen G, Dubois C, Cantelmo AR, et al. Role of glutamine synthetase in angiogenesis beyond glutamine synthesis. Nature. 2018;561(7721):63–9. https://doi.org/10.1038/s41586-018-0466-7.
28. Tibbetts AS, Appling DR. Compartmentalization of mammalian folate-mediated one-carbon metabolism. Annu Rev Nutr. 2010;30:57–81. https://doi.org/10.1146/annurev.nutr.012809.104810.
29. Preguiça I, Alves A, Nunes S, et al. Diet-induced rodent models of obesity-related metabolic disorders-A guide to a translational perspective. Obes Reviews: Official J Int Association Study Obes. 2020;21(12):e13081. https://doi.org/10.1111/obr.13081.
30. Della Torre S. Beyond the X factor: relevance of sex hormones in NAFLD Pathophysiology. Cells. 2021;10(9). https://doi.org/10.3390/cells10092502.
31. Castera L, Friedrich-Rust M, Loomba R. Noninvasive Assessment of Liver Disease in patients with nonalcoholic fatty liver disease. Gastroenterology. 2019;156(5):1264–e12811264. https://doi.org/10.1053/j.gastro.2018.12.036.
32. Targher G, Byrne CD, Tilg H. MASLD: a systemic metabolic disorder with cardiovascular and malignant complications. Gut. 2024;73(4):691–702. https://doi.org/10.1136/gutjnl-2023-330595.
33. Mantovani A, Petracca G, Beatrice G, et al. Non-alcoholic fatty liver disease and risk of incident diabetes mellitus: an updated meta-analysis of 501 022 adult individuals. Gut. 2021;70(5):962–9. https://doi.org/10.1136/gutjnl-2020-322572.
34. Friedman SL, Neuschwander-Tetri BA, Rinella M, et al. Mechanisms of NAFLD development and therapeutic strategies. Nat Med. 2018;24(7):908–22. https://doi.org/10.1038/s41591-018-0104-9.
35. Loomba R, Abdelmalek MF, Armstrong MJ, et al. Semaglutide 2·4 mg once weekly in patients with non-alcoholic steatohepatitis-related cirrhosis: a randomised, placebo-controlled phase 2 trial, the lancet. Gastroenterol Hepatol. 2023;8(6):511–22. https://doi.org/10.1016/s2468-1253(23)00068-7.
36. Harrison SA, Rolph T, Knot M, et al. FGF21 agonists: an emerging therapeutic for metabolic dysfunction-Associated Steatohepatitis and Beyond. J Hepatol. 2024. https://doi.org/10.1016/j.jhep.2024.04.034.
37. Rosenstock J, Wysham C, Frías JP, et al. Efficacy and safety of a novel dual GIP and GLP-1 receptor agonist tirzepatide in patients with type 2 diabetes (SURPASS-1): a double-blind, randomised, phase 3 trial. Lancet (London England). 2021;398(10295):143–55. https://doi.org/10.1016/s0140-6736(21)01324-6.
38. Ying Z, van Eenige R, Ge X, et al. Combined GIP receptor and GLP1 receptor agonism attenuates NAFLD in male APOE*3-Leiden.CETP mice. EBioMedicine. 2023;93:104684. https://doi.org/10.1016/j.ebiom.2023.104684.
39. Secher A, Jelsing J, Baquero AF, et al. The arcuate nucleus mediates GLP-1 receptor agonist liraglutide-dependent weight loss. J Clin Investig. 2014;124(10):4473–88. https://doi.org/10.1172/jci75276.
40. Gabery S, Salinas CG, Paulsen SJ, et al. Semaglutide lowers body weight in rodents via distributed neural pathways. JCI Insight. 2020;5(6). https://doi.org/10.1172/jci.insight.133429.
41. Harada N, Inagaki N. Role of GIP receptor signaling in β-cell survival. Diabetol Int. 2017;8(2):137–8. https://doi.org/10.1007/s13340-017-0317-z.
42. Frias JP, Bastyr EJ 3rd, Vignati L, et al. The Sustained effects of a dual GIP/GLP-1 receptor agonist, NNC0090-2746, in patients with type 2 diabetes. Cell Metabol. 2017;26(2):343–e352342. https://doi.org/10.1016/j.cmet.2017.07.011.
43. Liu Z, Liu M, Fan M, et al. Metabolomic-proteomic combination analysis reveals the targets and molecular pathways associated with hydrogen sulfide alleviating NAFLD. Life Sci. 2021;264:118629. https://doi.org/10.1016/j.lfs.2020.118629.
44. Zhao L, Zhang C, Luo X, et al. CD36 palmitoylation disrupts free fatty acid metabolism and promotes tissue inflammation in non-alcoholic steatohepatitis. J Hepatol. 2018;69(3):705–17. https://doi.org/10.1016/j.jhep.2018.04.006.
45. Rao MS, Reddy JK. Peroxisomal beta-oxidation and steatohepatitis. Semin Liver Dis. 2001;21(1):43–55. https://doi.org/10.1055/s-2001-12928.
46. Ipsen DH, Lykkesfeldt J, Tveden-Nyborg P. Molecular mechanisms of hepatic lipid accumulation in non-alcoholic fatty liver disease. Cell Mol life Sci : CMLS. 2018;75(18):3313–27. https://doi.org/10.1007/s00018-018-2860-6.
47. Baechler BL, Bloemberg D, Quadrilatero J. Mitophagy regulates mitochondrial network signaling, oxidative stress, and apoptosis during myoblast differentiation. Autophagy. 2019;15(9):1606–19. https://doi.org/10.1080/15548627.2019.1591672.
48. Alexander CC, Munkáscy E, Tillmon H et al. HspB1 overexpression improves life span and Stress Resistance in an invertebrate model, the journals of gerontology. Series A, Biological sciences and medical sciences 77 (2) (2022) 268–75, https://doi.org/10.1093/gerona/glab296
49. Du D, Liu C, Qin M, et al. Metabolic dysregulation and emerging therapeutical targets for hepatocellular carcinoma. Acta Pharm Sinica B. 2022;12(2):558–80. https://doi.org/10.1016/j.apsb.2021.09.019.
50. Picca A, Faitg J, Auwerx J, et al. Mitophagy in human health, ageing and disease. Nat Metabolism. 2023;5(12):2047–61. https://doi.org/10.1038/s42255-023-00930-8.
51. Begriche K, Massart J, Robin MA, et al. Mitochondrial adaptations and dysfunctions in nonalcoholic fatty liver disease. Hepatology (Baltimore MD). 2013;58(4):1497–507. https://doi.org/10.1002/hep.26226.
52. Nassir F, Ibdah JA. Role of mitochondria in nonalcoholic fatty liver disease. Int J Mol Sci. 2014;15(5):8713–42. https://doi.org/10.3390/ijms15058713.
53. Yim WW, Mizushima N. Lysosome biology in autophagy. Cell Discovery. 2020;6:6. https://doi.org/10.1038/s41421-020-0141-7.
54. Chang TM, Chi MC, Chiang YC, et al. Promotion of ROS-mediated apoptosis, G2/M arrest, and autophagy by naringenin in non-small cell lung cancer. Int J Biol Sci. 2024;20(3):1093–109. https://doi.org/10.7150/ijbs.85443.
55. Zhang XW, Zhou JC, Peng D, et al. Disrupting the TRIB3-SQSTM1 interaction reduces liver fibrosis by restoring autophagy and suppressing exosome-mediated HSC activation. Autophagy. 2020;16(5):782–96. https://doi.org/10.1080/15548627.2019.1635383.
56. Li Y, Xu J, Chen W, et al. Hepatocyte CD36 modulates UBQLN1-mediated proteasomal degradation of autophagic SNARE proteins contributing to septic liver injury. Autophagy. 2023;19(9):2504–19. https://doi.org/10.1080/15548627.2023.2196876.
57. Chen Q, Kou H, Demy DL et al. The different roles of V-ATPase a subunits in phagocytosis/endocytosis and autophagy, Autophagy (2024) 1–17, https://doi.org/10.1080/15548627.2024.2366748
58. Zhang J, Zeng W, Han Y, et al. Lysosomal LAMP proteins regulate lysosomal pH by direct inhibition of the TMEM175 channel. Mol Cell. 2023;83(14):2524–e25392527. https://doi.org/10.1016/j.molcel.2023.06.004.
59. Zhang W, Yang X, Li Y, et al. GCAF(TMEM251) regulates lysosome biogenesis by activating the mannose-6-phosphate pathway. Nat Commun. 2022;13(1):5351. https://doi.org/10.1038/s41467-022-33025-1.
60. Sayin SI, Wahlström A, Felin J, et al. Gut microbiota regulates bile acid metabolism by reducing the levels of tauro-beta-muricholic acid, a naturally occurring FXR antagonist. Cell Metabol. 2013;17(2):225–35. https://doi.org/10.1016/j.cmet.2013.01.003.
61. Y L. - hepatocyte CD36 modulates UBQLN1-mediated proteasomal degradation of autophagic. - Autophagy. 2023;19(9):2504–19. Epub (– 1554–8635 (Electronic)) – 2504–2519,.
62. Fleishman JS, Kumar S. Bile acid metabolism and signaling in health and disease: molecular mechanisms and therapeutic targets. Signal Transduct Target Therapy. 2024;9(1):97. https://doi.org/10.1038/s41392-024-01811-6.

63. Wang JQ, Li LL, Hu A, et al. Inhibition of ASGR1 decreases lipid levels by promoting cholesterol excretion. Nature. 2022;608(7922):413–20. https://doi.org/10.1038/s41586-022-05006-3.

Publisher's note